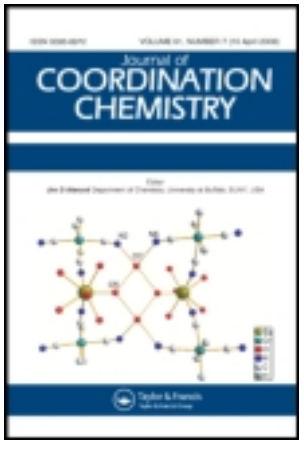

Journal of Coordination Chemistry
Publication details, including instructions for authors and subscription information:
http://www.tandfonline.com/loi/gcoo20

Syntheses, crystal structures, and magnetic properties of two new manganese(II) complexes based on biphenyl-2,5,2′,5′-tetracarboxylic acid

Dan Tian [a], Yu Pang [a], Shengqi Guo [a], Xiaofei Zhu [a] & Hong Zhang [a]

[a] Department of Chemistry, Institute of Polyoxometalate Chemistry, Northeast Normal University, Changchun, Jilin 130024, P.R. China

Published online: 03 Mar 2011.

To cite this article: Dan Tian, Yu Pang, Shengqi Guo, Xiaofei Zhu & Hong Zhang (2011) Syntheses, crystal structures, and magnetic properties of two new manganese(II) complexes based on biphenyl-2,5,2′,5′-tetracarboxylic acid, Journal of Coordination Chemistry, 64:6, 1006-1015, DOI: 10.1080/00958972.2011.560941

To link to this article: http://dx.doi.org/10.1080/00958972.2011.560941

Journal of Coordination Chemistry
Vol. 64, No. 6, 20 March 2011, 1006–1015

Syntheses, crystal structures, and magnetic properties of two new manganese(II) complexes based on biphenyl-2,5,2′,5′-tetracarboxylic acid

DAN TIAN, YU PANG, SHENGQI GUO, XIAOFEI ZHU and HONG ZHANG*

Department of Chemistry, Institute of Polyoxometalate Chemistry,
Northeast Normal University, Changchun, Jilin 130024, P.R. China

(*Received 4 November 2010; in final form 17 December 2010*)

Two new complexes, $[Mn(H_2bptc)(2,2'\text{-bpy})_2]\cdot 2H_2O$ (**1**) and $[Mn_3(Hbptc)_2(2,2'\text{-bpy})_3(H_2O)_8]\cdot 2H_2O$ (**2**) (H_4bptc = biphenyl-2,5,2′,5′-tetracarboxylic acid, 2,2′-bpy = 2,2′-bipyridine), have been synthesized under hydrothermal conditions. Their structures have been characterized by single-crystal X-ray diffraction, elemental analyses, IR spectra, powder X-ray diffraction, and thermogravimetric analyses. Complexes **1** and **2** are both linked into 3-D supramolecular networks by non-covalent interactions (O–H $\cdots$ O, C–H $\cdots$ O, C–H $\cdots$ π, and $\pi \cdots \pi$). Complexes **1** and **2** exhibit weak antiferromagnetic interactions.

Keywords: Manganese(II) complexes; Biphenyl-2,5,2′,5′-tetracarboxylic acid; Supramolecular structure; Antiferromagnetic interactions

1. Introduction

Design and synthesis of supramolecular coordination polymeric networks, especially those constructed by hydrogen-bonding and $\pi \cdots \pi$ stacking interactions have been a field of rapid growth due to their potential applications as functional materials [1, 2]. Hydrogen bonding is readily formed between carboxylate and H-donors, which can cross-link into a higher-dimensional and more stabilized structure [3, 4]. Multicarboxylate ligands have been proven to be good candidates, because they can be regarded not only as hydrogen-bond acceptors but also as hydrogen-bond donors [5]. We are interested in complexes constructed from flexible carboxylates and transition metals. Various tetracarboxylate ligands, such as pyrazine-2,3,5,6-tetracarboxylic acid [6, 7], 3,4,3′,4′-benzophenone-tetracarboxylate [8–10], biphenyl-2,3,2′,3′-tetracarboxylic acid [11, 12], and benzene-1,2,4,5-tetracarboxylate [13, 14], have been used to produce metal–organic coordination frameworks. However, biphenyl-2,2′,5,5′-tetracarboxylic acid (H_4bptc) is rarely used [15, 16]; it has four carboxyl groups that may be completely or partially deprotonated to generate H_3bptc^-, H_2bptc^{2-}, $Hbptc^{3-}$, or $bptc^{4-}$, depending

*Corresponding author. Email: zhangh@nenu.edu.cn

Journal of Coordination Chemistry
ISSN 0095-8972 print/ISSN 1029-0389 online
DOI: 10.1080/00958972.2011.560941

on the pH and also because two phenyl rings of the flexible ligand can be rotated around the C–C single bond.

We chose biphenyl-2,5,2′,5′-tetracarboxylic acid (H_4bptc) as multidentate O-donors. Five complexes of biphenyl-2,5,2′,5′-tetracarboxylic acid, which possess good magnetic and luminescent properties, have been prepared by our group [17]. Herein, we report the syntheses, crystal structures, IR spectra, powder X-ray diffraction (PXRD), thermogravimetric analyses (TGA), and magnetic properties of two supramolecular complexes $[Mn(H_2bptc)(2,2'\text{-bpy})_2]\cdot 2H_2O$ (**1**) and $[Mn_3(Hbptc)_2(2,2'\text{-bpy})_3(H_2O)_8]\cdot 2H_2O$ (**2**).

2. Experimental

2.1. *Materials and physical measurements*

All reagents were purchased commercially and were used without purification. The FT-IR spectra were recorded using KBr pellets from 4000 to 400 cm^{-1} on a Mattson Alpha-Centauri spectrometer. Elemental analyses for C, H, and N were performed on a Perkin-Elmer 2400 elemental analyzer. PXRD patterns were collected on a Rigaku D_{max} 2550 X-ray diffractometer with graphite-monochromated high-intensity Cu-Kα radiation ($\lambda = 0.154$ nm) and 2θ ranging from 5° to 50°. The thermal behaviors were studied by TGA on a Perkin-Elmer thermal analyzer under N_2 with a heating rate of 10°C min^{-1}. The temperature-dependent magnetic susceptibilities were measured with crystalline samples on a Quantum Design MPMS XL-5 Squid magnetometer in a magnetic field of 1000 Oe from 2 to 300 K.

2.2. *Synthesis of $[Mn(H_2bptc)(2,2'\text{-bpy})_2]\cdot 2H_2O$ (1)*

A mixture of $MnCl_2\cdot 4H_2O$ (9.9 mg, 0.05 mmol), H_4bptc (16.5 mg, 0.05 mmol), 2,2′-bpy (15.62 mg, 0.10 mmol), and H_2O (20 mL) was adjusted to pH 6.0 with 0.10 mol L^{-1} NaOH solution, sealed in a 25 mL Teflon reactor and heated at 150°C for 96 h. After the sample cooled to room temperature at a rate of 5°C h^{-1}, yellow needle-shaped crystals were obtained. Yield: 51% based on Mn(II) salt. Anal. Calcd for $C_{36}H_{28}MnN_4O_{10}$ (%): C, 59.10; H, 3.86; N, 7.66. Found (%): C, 59.15; H, 3.96; N, 7.58. IR (KBr, cm^{-1}): 3859s, 3742s, 3673s, 3649s, 3624s, 3393w, 3060 m, 1741s, 1700s, 1653s, 1597s, 1560s, 1508s, 1438s, 1379 m, 1229s, 1156s, 1114s, 1010s, 833s, 759s, 674s, 646s, 477s, 425s.

2.3. *Synthesis of $[Mn_3(Hbptc)_2(2,2'\text{-bpy})_3(H_2O)_8]\cdot 2H_2O$ (2)*

The preparation of **2** was similar to that of **1** except that the molar ratio of $MnCl_2\cdot 4H_2O$, H_4bptc, 2,2′-bpy was changed to 3 : 2 : 3 and the pH of the mixture was changed to 7.0. Yellow block-shaped crystals of **2** were obtained. Yield: 45% based on Mn(II) salts. Anal. Calcd for $C_{62}H_{58}Mn_3N_6O_{26}$ (%): C, 50.72; H, 3.98; N, 5.72. Found (%): C, 50.33; H, 4.07; N, 5.88. IR (KBr, cm^{-1}): 3564w, 3477w, 3413s, 3064w,

Table 1. Details of crystal data and structure refinement parameters for **1** and **2**.

Complex	**1**	**2**
Empirical formula	$C_{36}H_{28}MnN_4O_{10}$	$C_{62}H_{58}Mn_3N_6O_{26}$
Formula weight	731.56	1467.96
Temperature (K)	293(2)	293(2)
Wavelength λ (Å)	0.71073	0.71073
Crystal system	Triclinic	Monoclinic
Space group	$P\bar{1}$	$C2/c$
Unit cell dimensions (Å, °)		
a	9.5257(16)	20.194(3)
b	9.6749(16)	12.989(3)
c	20.999(4)	24.080(5)
α	95.684(3)	90
β	90.154(3)	102.025(4)
γ	119.089(2)	90
Volume (Å^3), Z	1680.0(5), 2	6178.2, 4
Calculated density (g cm^{-3})	1.446	1.570
Absorption coefficient (mm^{-1})	0.459	0.697
F(000)	754.0	2988.0
R_{int}	0.0310	0.0726
Goodness-of fit on F^2	1.014	1.020
Final R indices [$I > 2\sigma(I)$]	$R_1 = 0.0629$, $wR_2 = 0.1346$	$R_1 = 0.0506$, $wR_2 = 0.1157$

$R_1 = \Sigma||F_o| - |F_c||/\Sigma|F_o|$, $wR_2 = \Sigma\{[w(F_o^2 - F_c^2)^2]/\ \Sigma[w(F_o^2)]^2\}^{1/2}$.

1650s, 1625s, 1590s, 1497s, 1481s, 1346s, 1256s, 1180s, 933s, 867s, 844s, 727s, 640s, 556s.

2.4. *X-ray crystallography*

Single-crystal X-ray diffraction data for **1** and **2** were recorded on a Bruker Apex CCD diffractometer with graphite-monochromated Mo-Kα radiation (λ = 0.71073 Å) at 293 K. Absorption corrections were performed empirically. The structures were solved by direct methods followed by difference Fourier and refined by full-matrix least-squares on F^2 using SHELXS-97 and SHELXL-97 [18]. All non-hydrogen atoms were refined anisotropically; hydrogens of organic ligand are located geometrically. Hydrogens of water were located from difference Fourier maps. The crystal data and structure refinements of **1** and **2** are summarized in table 1 and selected bond lengths and angles are listed in table 2, while O–H···O, C–H···O, C–H···π, and π···π interactions in **1** and **2** are listed in table S1.

3. Results and discussion

3.1. *Crystal structure of 1*

Structure analysis reveals that **1** crystallizes in the triclinic space group $P\bar{1}$. The asymmetric unit consists of one Mn(II), one H_2bptc^{2-} anion, two 2,2′-bpy molecules, and two guest waters. As depicted in figure 1a, each Mn(II) is coordinated by

Table 2. Selected bond lengths (Å) and angles (°) for **1** and **2**.

$[Mn(H_2bptc)(2,2'\text{-bpy})_2]\cdot 2H_2O$ (**1**)			
Mn1–O2	2.117(3)	N3–Mn1–N1	162.37(17)
Mn1–O1	2.143(3)	O2–Mn1–N4	83.05(15)
Mn1–N3	2.245(5)	O1–Mn1–N4	160.68(15)
Mn1–N1	2.265(5)	N3–Mn1–N4	71.73(17)
Mn1–N4	2.273(5)	N1–Mn1–N4	97.37(17)
Mn1–N2	2.287(5)	O2–Mn1–N2	158.50(17)
O2–Mn1–O1	102.97(13)	O1–Mn1–N2	86.14(15)
O2–Mn1–N3	104.14(16)	N3–Mn1–N2	95.35(19)
O1–Mn1–N3	88.97(15)	N1–Mn1–N2	71.26(18)
O2–Mn1–N1	87.76(15)	N4–Mn1–N2	94.76(17)
O1–Mn1–N1	101.17(15)		
$[Mn_3(Hbptc)_2(2,2'\text{-bpy})_3(H_2O)_8]\cdot 2H_2O$ (**2**)			
Mn1–O1#1	2.105(2)	O1W#1–Mn1–N3	86.70(13)
Mn1–O1	2.105(2)	O1#1–Mn1–N3#1	164.61(11)
Mn1–O1W	2.212(3)	O1–Mn1–N3#1	93.55(11)
Mn1–O1W#1	2.212(3)	O1W–Mn1–N3#1	86.70(13)
Mn1–N3	2.287(3)	O1W#1–Mn1–N3#1	84.79(12)
Mn1–N3#1	2.287(3)	N3–Mn1–N3#1	71.95(17)
Mn2–O4	2.122(3)	O4–Mn2–O2W	89.18(13)
Mn2–O2W	2.160(3)	O4–Mn2–O3W	109.17(11)
Mn2–O3W	2.178(3)	O2W–Mn2–O3W	88.19(13)
Mn2–O4W	2.224(3)	O4–Mn2–O4W	88.46(12)
Mn2–N1	2.254(3)	O2W–Mn2–O4W	168.60(13)
Mn2–N2	2.321(3)	O3W–Mn2–O4W	82.05(13)
O1#1–Mn1–O1	101.31(14)	O4–Mn2–N1	88.17(11)
O1#1–Mn1–O1W	86.84(11)	O2W–Mn2–N1	90.24(12)
O1–Mn1–O1W	99.86(11)	O3W–Mn2–N1	162.56(12)
O1#1–Mn1–O1W#1	99.87(12)	O4W–Mn2–N1	100.83(13)
O1–Mn1–O1W#1	86.84(11)	O4–Mn2–N2	155.98(11)
O1W–Mn1–O1W#1	169.48(17)	O2W–Mn2–N2	102.07(13)
O1#1–Mn1–N3	93.55(11)	O3W–Mn2–N2	92.51(12)
O1–Mn1–N3	164.61(11)	O4W–Mn2–N2	84.33(13)
O1W–Mn1–N3	84.79(12)	N1–Mn2–N2	70.84(12)

Symmetry codes: #1: $-x+2$, y, $-z+1/2$.

two oxygens (O1 and O2) from two carboxyl groups of one H_2bptc^{2-} and four nitrogens from two 2,2′-bpy ligands, resulting in a slightly distorted MnN_4O_2 octahedral geometry. The 2 and 2′-carboxylates of H_2bptc^{2-} in **1** display monodentate coordination (Chart 1a) with O1 and O2 fulfilling the coordination of Mn and the other oxygens remain uncoordinated.

Careful inspection of the crystal structure reveals that the 2-D structure (figure 1b) in **1** is stabilized by O–H···O interactions (O6···O3 2.556 Å, O7···O4 2.612 Å, table S1) between different carboxyl groups and $\pi\cdots\pi$ stacking interactions between adjacent pyridine rings and benzene rings with centroid-to-centroid distance of 3.842 Å (table S1). Adjacent 2-D layers are further assembled through O–H···O interactions (O1W···O3 2.883 Å, O1W···O5 2.898 Å, O2W···O8 3.077 Å, O2W···O4 3.034 Å, table S1) between water and carboxyl groups and C–H···O interactions (C12···O2W 3.315 Å, C24···O1W 3.336 Å, table S1) between aromatic ring protons and non-coordinated water to generate a 3-D supramolecular structure (figure 1c). It is clear that water plays an important role in the formation of the 3-D framework.

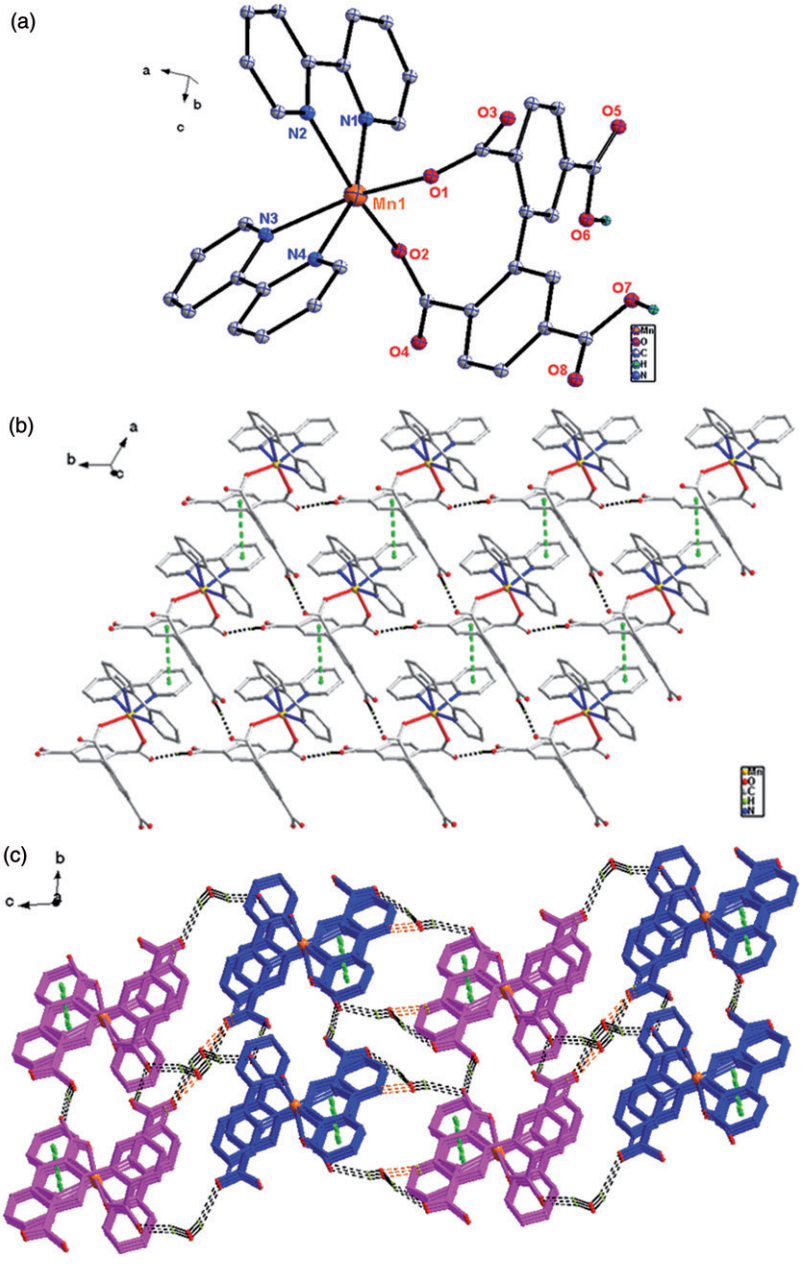

Figure 1. (a) Coordination environment of Mn in **1**; (b) perspective view of the 2-D layer formed *via* O–H $\cdots$ O (black dotted lines) and $\pi \cdots \pi$ (bright green dotted lines) interactions in **1**; (c) perspective view of the 3-D supramolecular network stabilized by O–H $\cdots$ O (black dotted lines), C–H $\cdots$ O (orange dotted lines), and $\pi \cdots \pi$ (bright green dotted lines) interactions in **1**; the 2-D layers are highlighted with different colors.

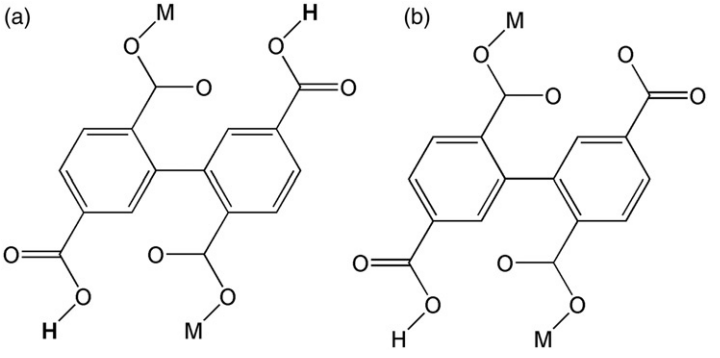

Chart 1. The coordination modes for (a) H_2bptc^{2-} and (b) $Hbptc^{3-}$.

3.2. *Crystal structure of 2*

When we change the molar ratio of the materials and pH, a different 0-D complex is formed. Complex **2** crystallizes in the monoclinic space group *C2/c*. The asymmetric unit consists of one half Mn(II), one $Hbptc^{3-}$, one half 2,2′-bpy, four coordination waters, and one guest water. As depicted in figure 2a, Mn1 lies in a distorted MnN_2O_4 octahedral environment, defined by two nitrogens (N3 and N3#) from one 2,2′-bpy and two carboxylate oxygens (O1 and O1#) from two different $Hbptc^{3-}$ in the equatorial positions; axial positions are occupied by two terminal waters (O1W and O1W#). The six-coordinate Mn2 has a slightly distorted octahedral geometry surrounded by two nitrogens (N1 and N2) from one 2,2′-bpy, one coordination water (O3W), one carboxylate oxygen (O4) from one $Hbptc^{3-}$ in the equatorial plane and two coordination waters (O2W and O4W) at axial positions. In the unit cell of **2**, three Mn(II) ions are linked by two $Hbptc^{3-}$ through four monodentate carboxylates, giving Mn1 $\cdots$ Mn2 and Mn2 $\cdots$ Mn2 distances of 6.801 and 10.108 Å, respectively. The $Hbptc^{3-}$ in **2** adopt analogous coordination mode (Chart 1b) with **1**.

Similar to **1**, the 3-D supramolecular network of **2** is also assembled by non-covalent interactions. The 2-D undulating layer (figure 2b) is formed *via* three types of interactions. The first is O–H $\cdots$ O interactions (O4W $\cdots$ O5 2.854 Å, O2W $\cdots$ O7 2.674 Å, O1W $\cdots$ O5 2.804 Å, O5W $\cdots$ O2 2.882 Å, O5W $\cdots$ O8 2.730 Å, table S1) between the water and carboxylic acid moieties; the second is C–H $\cdots$ π interactions between pyridine ring protons and benzene rings with the edge-to-face separation of 2.86 Å (table S1); the third is $\pi \cdots \pi$ stacking interactions between adjacent pyridine rings with the centroid-to-centroid distance of 3.658 Å (table S1). The 2-D supramolecular sheets are held together *via* strong O–H $\cdots$ O interactions (O3W $\cdots$ O3 2.671 Å, O6 $\cdots$ O5W 2.574 Å, O4W $\cdots$ O3W 2.937 Å, O4W $\cdots$ O5W 3.083 Å, O3W $\cdots$ O8 2.649 Å, table S1), generating a 3-D supramolecule framework (figure 2c). Obviously, O–H $\cdots$ O, C–H $\cdots$ π, and $\pi \cdots \pi$ stacking interactions play important roles in stabilizing the 3-D supramolecular architecture.

In **1** and **2**, H_2bptc^{2-} and $Hbptc^{3-}$ show torsion with dihedral angles between two benzene rings being *ca* 65.03 and 50.02°, respectively. The 2-, 2′-, 5-, and 5′-carboxylates of H_2bptc^{2-} in **1** have dihedral angles 48.42°, 53.41°, 9.26°, and 15.40°, respectively,

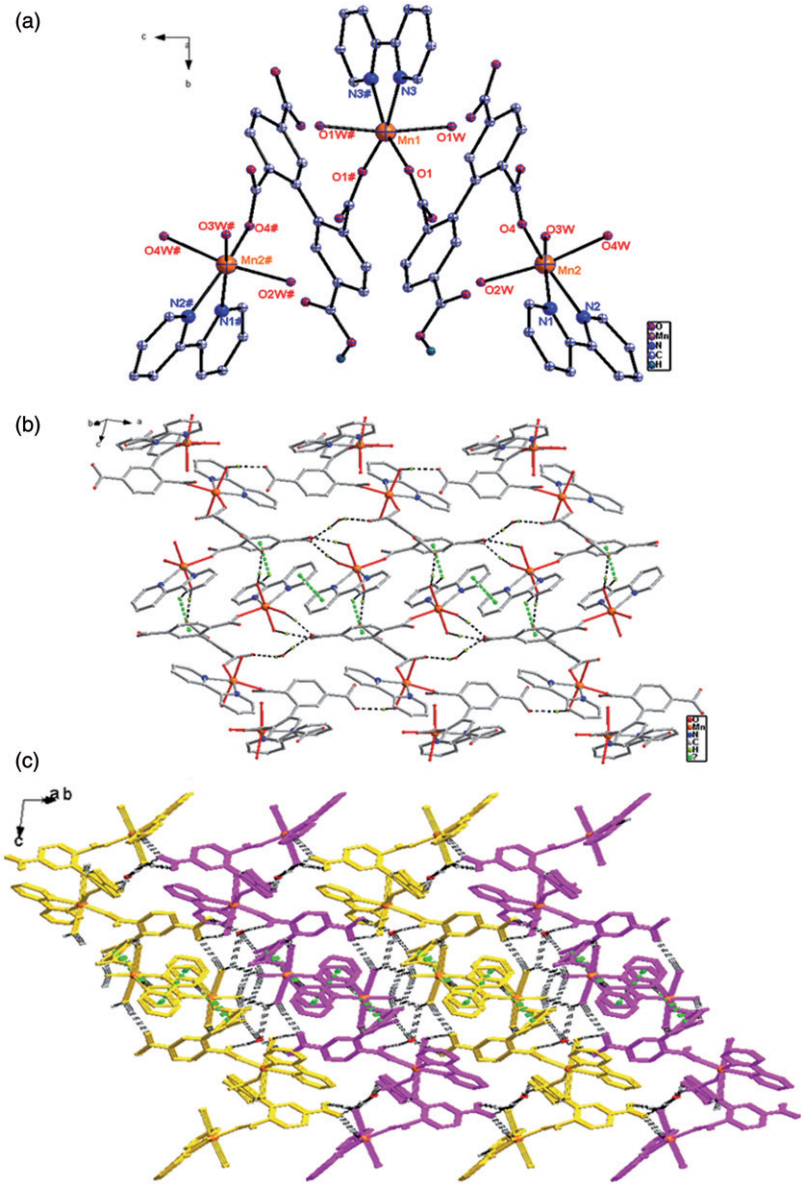

Figure 2. (a) The coordination environment of Mn in **2**. Symmetry codes: #: $-x+2$, y, $-z+1/2$; (b) a view of a 2-D structure formed *via* O–H $\cdots$ O (black dotted lines), C–H $\cdots$ π and $\pi \cdots \pi$ (bright green dotted lines) interactions in **2**; (c) perspective view of the 3-D supramolecular structure stabilized by O–H $\cdots$ O (black dotted lines), C–H $\cdots$ π, and $\pi \cdots \pi$ (bright green dotted lines) interactions in **2**; the 2-D layers are highlighted with different colors.

with the plane of corresponding linking phenyl rings; for $Hbptc^{3-}$ in **2**, those angles are 40.00°, 58.42°, 16.81°, and 3.75°, respectively. The Mn–O and Mn–N bond distances of **1** and **2** fall in the range 2.105(2)~2.224(3) and 2.245(5)~2.321(3) Å, respectively, in agreement with those of Mn(II) analogues with 2,2′-bpy [19–21].

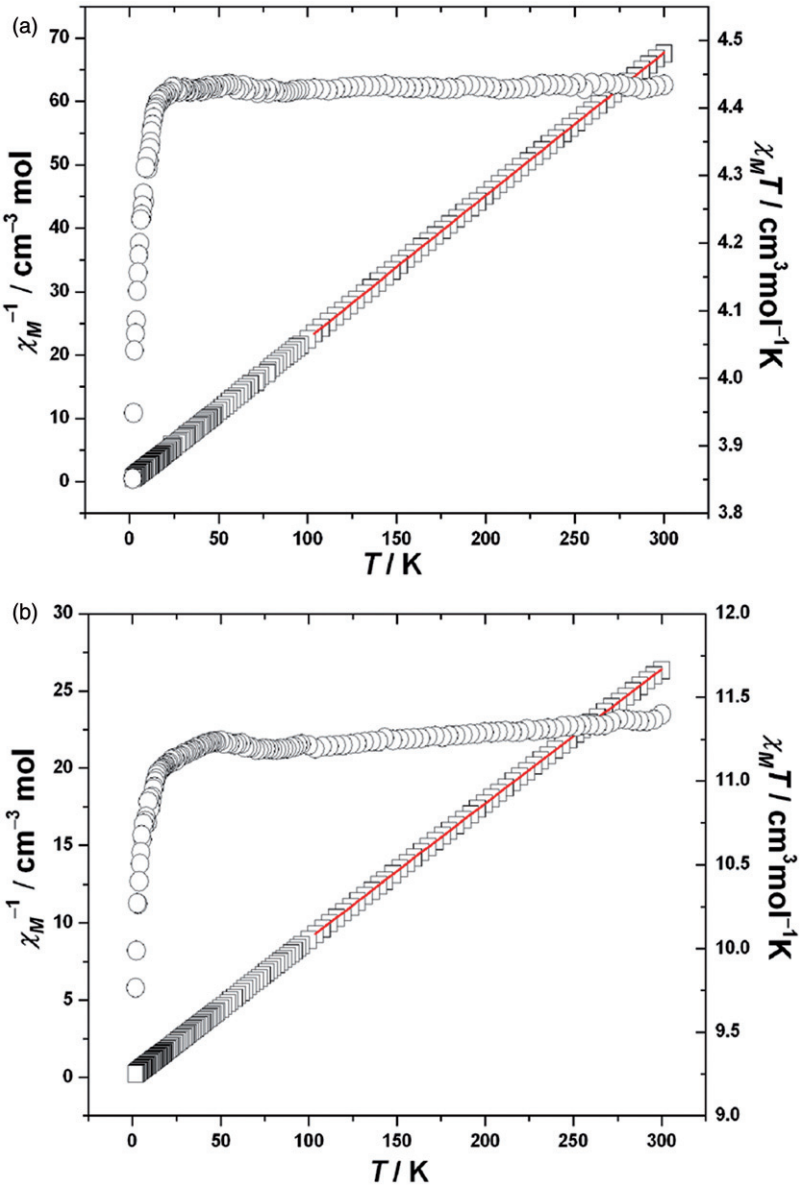

Figure 3. Plots of the temperature dependence of $\chi_M T$ and χ_M^{-1} for (a) **1** and (b) **2** at 2–300 K.

3.3. *Magnetic measurements*

Solidstate magnetic susceptibility measurements for **1** and **2** were performed from 2 to 300 K under a field of 1000 Oe, and plots of $\chi_M T$ and χ_M^{-1} *versus* T, where χ_M is the molar magnetic susceptibility, are shown in figures 3a and 3b. For **1**, the $\chi_M T$ value at 300 K is 4.433 cm^3 mol^{-1} K, slightly higher than the spin-only value of 4.375 cm^3 mol^{-1} K per Mn(II) ion (S = 5/2). Upon cooling, $\chi_M T$ decreases to

$3.851\,cm^3\,mol^{-1}\,K$ at 2 K. The decrease in the $\chi_M T$ is likely due to zero-field splitting (ZFS) [22, 23] of $S = 5/2$ and/or weak antiferromagnetic interactions. The fitting of the curve for the χ_M^{-1} *versus* T plot to the Curie–Weiss law [$\chi_M = C/(T - \theta)$] gives a good result in the temperature range 100–300 K with $C = 4.436\,cm^3\,mol^{-1}\,K$ and $\theta = -0.211$ K, consistent with the presence of weak antiferromagnetic interactions in **1**.

Complex **2** exhibits similar magnetic behavior. For **2**, at 300 K, $\chi_M T$ is $11.397\,cm^3\,mol^{-1}\,K$, which is lower than the calculated value of $13.125\,cm^3\,mol^{-1}\,K$ for three isolated spin-only Mn(II) ions with S = 5/2. Upon lowering the temperature, $\chi_M T$ smoothly decreases from 11.397 to $11.103\,cm^3\,mol^{-1}\,K$ at 20 K and then decreases more rapidly, reaching a value of $9.765\,cm^3\,mol^{-1}\,K$ at 2 K. This suggests antiferromagnetic interactions [24] between the metal centers probably assigned to zero-field splitting [22] and/or intermolecular interactions. The χ_M^{-1} *versus* T curve is well fitted by the Curie-Weiss law with the Curie constant of $11.465\,cm^3\,mol^{-1}\,K$ and Weiss temperature of −2.910 K, respectively. The small Weiss value is indicative of weak antiferromagnetic interactions between neighboring Mn(II) ions, possibly due to a long Mn···Mn distance of 6.801 Å.

3.4. *Thermal analyses*

The thermal stabilities of **1** and **2** were studied by TGA and are recorded in figure S1. For **1**, the first weight loss of 5.28% occurred at 100°C, corresponding to the release of H_2O (Calcd 4.93%), and the second step from 200°C to 443°C is due to the release of organic species (Obsd. 87.88%, Calcd 87.94%). The TG curve of **2** exhibits three steps of weight loss, giving a total weight loss of 90.70% (Calcd 89.00%) in the range 100–600°C. The first two weight losses are 2.73% and 9.99% in the ranges 100–140°C and 140–170°C, respectively, which correspond to the loss of lattice and coordinated water (Calcd 2.45% and 9.80%). The third weight loss of 77.98% at 287–600°C is assigned to decomposition of organic ligands (Calcd 76.75%).

3.5. *PXRD measurement*

The simulated and experimental PXRD patterns of **1** and **2** are in agreement with each other (figure S2) excluding a few unaccounted peaks. The unaccounted peaks and the differences in intensity may be due to a small quantity of impurity phase and the preferred orientation of the powder samples. Moreover, the impurity phase may have impact on thermal and magnetic properties.

4. Conclusion

We synthesized two new Mn(II) complexes based on tetracarboxylate and 2,2′-bpy under hydrothermal conditions. They were formed under similar reaction conditions but with different molar ratio of the materials and pH. The result of this study illustrates that the molar ratio of the materials and pH of the mixture affect the structures of the complexes. The complexes show weak antiferromagnetic interactions.

Further work toward constructing more coordination polymers based on biphenyl-2,5,2′,5′-tetracarboxylic acid is in progress.

Supplementary material

Crystallographic data for the structural analyses have been deposited with the Cambridge Crystallographic Data Center, CCDC Nos. 735917 and 763204 for **1** and **2**. Copies of this information may be obtained free of charge from The Director, CCDC, 12 Union Road, Cambridge CB21EZ, UK (Fax: +44-1223-336033; E-mail: deposit@ccdc.cam.ac.uk or http://www.ccdc.cam.ac.uk).

Acknowledgments

The authors gratefully acknowledge the financial support by the NSF of China (20771023), 863 Program (2007AA03z218) and analysis and testing foundation of Northeast Normal University.

References

[1] T.J. Barton, L.M. Bull, W.G. Klemperer, D.A. Loy, B. McEnaney, M. Misono, P.A. Monson, G. Pez, G.W. Scherer, J.C. Vartuli, O.M. Yaghi. *Chem. Mater*., **11**, 2633 (1999).
[2] Q. Shi, R. Cao, D.F. Sun, M.C. Hong, Y.C. Liang. *Polyhedron*, **20**, 3287 (2001).
[3] S.A. Dalrymple, G.K.H. Shimizu. *J. Am. Chem. Soc*., **129**, 12114 (2007).
[4] T.Z. Forbes, S.C. Sevov. *Inorg. Chem*., **48**, 6873 (2009).
[5] X.L. Wang, C. Qin, E.B. Wang. *Cryst. Growth Des*., **6**, 439 (2006).
[6] A.H. Yang, Y.P. Quan, L.H. Zhao, J.Z. Cui, H.L. Gao, F.L. Lu, W. Shi, P. Cheng. *J. Coord. Chem*., **62**, 3306 (2009).
[7] W. Starosta, J. Leciejewicz. *J. Coord. Chem*., **61**, 490 (2008).
[8] X. Zhuo, Z.W. Wang, Z.R. Pan, Y.Z. Li, H.G. Zheng. *J. Coord. Chem*., **61**, 1078 (2008).
[9] J.Q. Liu, Y.N. Zhang, Y.Y. Wang, J.C. Jin, E.K. Lermontova, Q.Z. Shi. *J. Chem. Soc., Dalton Trans*., 5365 (2009).
[10] J. Zhang, Z.J. Li, Y. Kang, J.K. Cheng, Y.G. Yao. *Inorg. Chem*., **43**, 8085 (2004).
[11] S.Q. Zang, Y. Su, Y.Z. Li, J.G. Lin, X.Y. Duan, Q.J. Meng, S. Gao. *CrystEngComm*., **11**, 122 (2009).
[12] S.Q. Zang, Y. Su, C.Y. Duan, Y.Z. Li, H.Z. Zhu, Q.J. Meng. *Chem. Commun*., 4997 (2006).
[13] H.Y. Lin, H.L. Hu, X.L. Wang, B. Mu, J. Li. *J. Coord. Chem*., **63**, 1295 (2010).
[14] D.P. Cheng, M.A. Khan, R.P. Houser. *Cryst. Growth Des*., **2**, 415 (2002).
[15] R.Z. Chen, F.J. Guo, F.L. Meng. *Acta Crystallogr., Sect. E*, **64**, m761 (2008).
[16] R.Z. Chen, F.J. Guo, F.L. Meng. *Acta Crystallogr., Sect. E*, **64**, m855 (2008).
[17] D. Tian, Y. Pang, Y.H. Zhou, L. Guan, H. Zhang. *CrystEngComm*., **13**, 957 (2011).
[18] G.M. Sheldrick. *SHELXS-97 and SHELXL-97, Programs for the Solution and Refinement of Crystal Structures*, University of Göttingen, Germany (1997).
[19] C.N. Chen, H.P. Zhu, D.G. Huang, T.B. Wen, Q.T. Liu, D.Z. Liao, J.Z. Cui. *Inorg. Chim. Acta*, **320**, 159 (2001).
[20] R.T.W. Scott, S. Parsons, M. Murugesu, W. Wernsdorfer, G. Christou, E.K. Brechin. *Chem. Commun*., 2083 (2005).
[21] X.M. Chen, K.L. Shi. *Acta Crystallogr., Sect. C*, **51**, 358 (1995).
[22] S. Naskar, D. Mishra, S.K. Chattopadhyay, M. Corbella, A.J. Blake. *J. Chem. Soc., Dalton Trans*., 2428 (2005).
[23] C.N. Chen, H.P. Zhu, D.G. Huang, T.B. Wen, Q.T. Liu, D.Z. Liao, J.Z. Cui. *Inorg. Chim. Acta*, **320**, 159 (2001).
[24] C.M. Qi, D. Zhang, S. Gao, H. Ma, Y. He, S.L. Ma, Y.F. Chen, X.J. Yang. *J. Mol. Struct*., **891**, 357 (2008).